IRON MINERALOGY AND REDOX CHEMISTRY OF THE MESOPROTEROZOIC NEWLAND FORMATION IN THE HELENA EMBAYMENT, BELT SUPERGROUP, MONTANA

Sarah P. Slotznick,[1*] Jerry Zieg,[2] Samuel M. Webb,[3] Joseph L. Kirschvink,[1,4] and Woodward W. Fischer[1]

*[1]Division of Geological and Planetary Sciences, California Institute of Technology, 1200 East California Boulevard, Pasadena, CA 91125, USA; [2]Tintina Resources Inc., 17 E. Main Street, P.O. Box 431, White Sulphur Springs, MT, 59645, USA;[3]Stanford Synchrotron Radiation Lightsource, Menlo Park, CA 94025, USA;[4]Earth-Life Science Institute, Tokyo Institute of Technology, Meguro-ku, Toyko 152-8550, Japan;*sslotz@caltech.edu*

INTRODUCTION

The Mesoproterozoic era falls in the period between 1.85 to 0.85 Ga called "the boring billion", sandwiched between the rise of multi-cellularity and animals in the Neoproterozoic and the Great Oxygenation Event and rise of oxygen in the Paleoproterozoic (Holland, 2006). However, important evolutionary developments occurred over the period with the rise of eukaryotes and macroscopic organisms (Knoll and others, 2006). The Belt Supergroup contains some of the early micro- and macrofossils that have been attributed to eukaryotes (Horodyski and others, 1989). One particularly well-studied example is found in the Greyson Shale of the Helena Embayment region in southwestern Montana (fig. 1a). First identified by Charles Doolittle Walcott (1899) and later renamed (Walter and others, 1976), Grypania spiralis is a curved or coiled ribbon, 0.2 to 1.7 mm wide, and 6 to 14 mm in coiled diameter, and has been interpreted as eukaryotic algae as well consortia of several microscopic organisms (Horodyski and others, 1989; Knoll and others, 2006; Walter and others, 1976).

Due to our understanding of eukaryotic phylogeny, the fact that most modern eukaryotes are aerobic, and the requirement of oxygen in making certain biological compounds (sterols) contained in eukaryotes, eukaryotes have been tied to oxygenic conditions (e.g. Brocks and others, 2003; Embley and Martin, 2006; Raymond and Blankenship, 2004). Therefore, there is a need to understand more about the environmental conditions in which early macroscopic organisms lived to understand the pacing of eukaryotic evolution and how it might have been aided, frustrated, or unaffected by changing environmental conditions during the Proterozoic.However, understanding the redox state of ancient oceans has been a longstanding problem since a good oxygen barometer has not yet been developed. In general, geologists and geochemists have looked at iron, sulfur, and other redox sensitive elements as records of oxygen levels, but these approaches often give discordant answers. Some studies have suggested a fully oxygenated mid-Proterozoic ocean (Cloud, 1968; Holland, 1984, 2006), while others have suggested a stratified system with anoxic and/or euxinic deep oceans (Canfield, 1998; Poulton and Canfield, 2011). Aerobic/oxic environments are defined as having >80 μM O2, anoxic/ferruginous have <5 μM O2, and euxinic environments are anoxic with H2S also present (Raiswell & Canfield 1998).

Even within the subset of studies focused on samples of the Belt Supergroup, there have been conflicting hypotheses about redox conditions. Due to their preservation and low metamorphic grade (Duke and Lewis, 2010), the strata contained in the Helena Embayment, specifically the shale-dominated Newland Formation, have been the main target for understanding the ancient redox character and geochemistry of the Belt Basin. Sulfate concentrations and sulfur isotopes (Gellatly and Lyons, 2005; Luepke and Lyons, 2001; Lyons and others, 2000) as well as presence of basin-wide sedimentary laminations in the shales of the Newland and Prichard Formations similar to those found in the Black Sea (Lyons and others, 2000) were initially argued as evidence of a chemically stratified euxinic basin during deposition of the lower Belt Supergroup. Bottom water suboxic to euxinic conditions were also suggested by the high (several wt.%) organic content observed in shales (Lyons and others, 2000), and the syndepositional to early diagenetic abundant pyrite and sulfide-hosted base metal deposits of Cu, Co, and Ag (Graham and others, 2012; White and others, 2014). Others suggested the euxinic conditions forming early diagenetic pyrite were restricted to pore waters (Schieber, 1989c).

In sharp contrast, iron speciation results indicate anoxic and ferruginous conditions for basinal waters of the lower Belt Supergroup (Planavsky and others, 2011). Iron speciation is a recently-developed bulk geochemical technique that uses sequential extraction to estimate proportions of different reactive iron minerals within a given rock sample (Poulton and Canfield, 2005), which are then mapped to redox conditions based on empirical calibrations from modern sediment samples. Additionally, recent nitrogen isotope measurements of samples from the Chamberlain, Greyson and Newland formations suggest oxygenated portions of the water column (Stüeken, 2013).

In this study, we focus on samples of the Newland Formation from the Black Butte Deposit in the Helena Embayment since previous workers investigating mid-Proterozoic redox conditions used drill core specimens from this deposit to avoid complications of recent surface oxidation (Gellatly and Lyons, 2005; Luepke and Lyons, 2001; Lyons and others, 2000; Planavsky and others, 2011). To help reconcile the different redox interpretations and test the iron speciation results, we investigated the iron mineralogy of the Newland Formation using a range of petrographic, spectroscopic, and rock magnetic techniques that help shed light on both the paleoenvironmental processes of iron deposition in the sediments as well as post-depositional modifications to those phases.

Bulk rock magnetism experiments provide sensitive techniques to identify ferromagnetic minerals, including magnetic iron sulfide phases. Magnetic iron sulfides such as pyrrhotite have not previously been identified in materials collected from the Newland Formation, but have been widely observed throughout correlative units elsewhere in the lower Belt Supergroup (e.g. Luepke, 1999; Luepke and Lyons, 2001; Slotznick and others, in review). Much of the pyrrhotite in the rock record is interpreted to be due to the metamorphic alteration of pyrite or precipitation from high temperature fluids (Craig and Vokes, 1993; Hall, 1986); and pyrrhotite observed in Belt strata reflects both of these post-depositional processes (Luepke, 1999). Pyrite can transform to pyrrhotite beginning at 200°C (Hall, 1986) if a suitable reducing environment or organic matter is present, although some experiments suggest even lower temperature transitions are possible (Moreau and others, 2005; Raub and others, 2012). Thus the presence of pyrrhotite can provide a tool for understanding metamorphic temperatures and metasomatic conditions of the Newland Formation at the Black Butte Deposit, aiding us in recognizing if bulk geochemical proxies have been compromised by post-depositional alteration.

Additionally, synchrotron-based X-ray spectroscopy provided a complimentary tool to discover and image a wide range of non-magnetic iron minerals such as chalcopyrite and pyrite while confirming the presence or absence of pyrrhotite. By applying these paired magnetic and spectroscopic techniques to the Belt Supergroup, we should be able to improve upon previous bulk geochemical studies in deducing how iron was being deposited and transformed in the environment to reconstruct ancient redox conditions.

GEOLOGIC SETTING

The Helena Embayment is an E-W trending limb of the larger Belt Basin, with strata broadly correlative to three of the four stratigraphic groups recognized elsewhere in the basin: lower Belt Group, Ravalli Group, Middle Belt Carbonate Group (fig. 1a; Graham and others, 2012; Winston and Link, 1993). Fine-grained siliciclastics and carbonates dominate the lower Belt in the northern part of the Helena Embayment near the Black Butte Deposit (fig. 1b). The Neihart Quartzite is a basal quartz arenite sandstone with planar and trough cross-bedding, parallel lamination, and lenses of pebbles lying unconformably on early Proterozoic gneiss basement (Schieber, 1989b; Walcott, 1899). Overlying the Neihart quartzite, the Chamberlain Formation is a wavy laminated to bedded black shale, siltstone and sandstone with lenses of molar tooth hash near the top (Zieg, 1986). The Chamberlain Formation grades into the Newland Formation. The Newland Formation varies considerably in thickness across the Embayment from 610 m to over 3000 m, but is approximately 1,100 m in the region of the Black Butte Cu-Co-Ag deposit near the northern margin of the Helena Embayment (Nelson, 1963; Walcott, 1899; Zieg, 1986).

The Newland Formation is subdivided into two informal members: a lower parallel-laminated shale interbedded with debris flows, turbidites, and carbonates and an upper shale with more abundant carbonate beds (Zieg, 1986). Conformably overlying the Newland Formation is the Greyson Formation of wavy

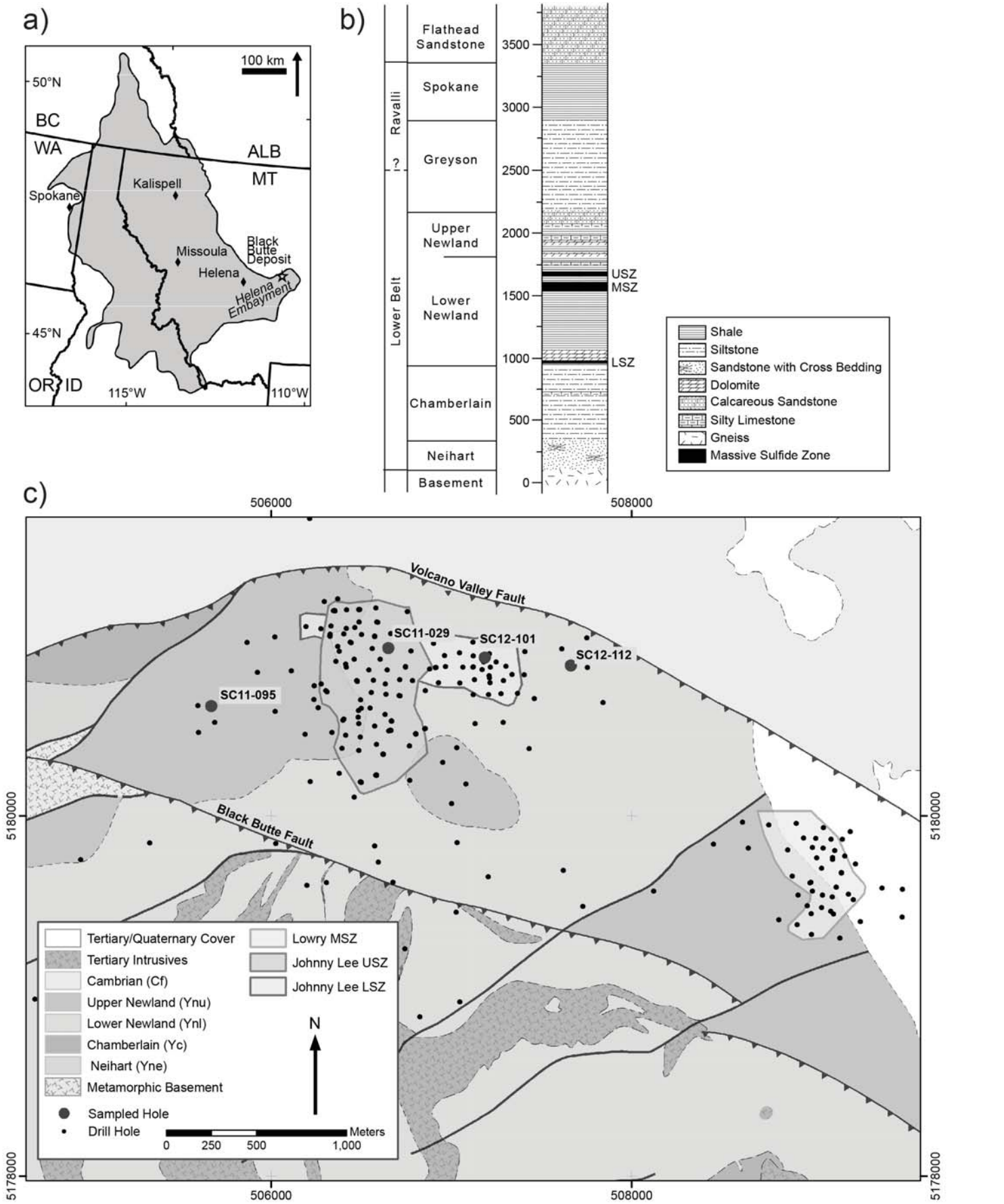

Figure 1. a) Map showing the extent of Belt Supergroup outcrops and the location of the Black Butte Deposit within the Helena Embayment. b) General stratigraphic column of Belt Supergroup strata in the Black Butte Deposit region of the Helena Embayment with height in meters. Note: USZ = Upper Sulfide Zone, MSZ = Middle Sulfide Zone, LSZ = Lower Sulfide Zone. c) Geologic Map of the Black Butte Deposit region with locations of all drill cores drilled by Tintina Resources Inc. and Cominco American Inc. and labels for the drill cores that were sampled in this study.

laminated siltstone and dark shale, which as been assigned by some to the lower Belt Group (Graham and others, 2012; Ross and Villeneuve, 2003; Winston and Link, 1993) and by others to the Ravalli Group (Harrison, 1972; Mudge and others, 1968). The red siltstone and claystone Spokane Formation overlies the Greyson Formation as part of the Ravalli Group. The Empire Formation (Ravalli Group) and the Helena Formation (Middle Belt Carbonate) are also exposed in the Helena Embayment, but these two units are not present in the Black Butte region. Instead, the Spokane is uncomfortably overlain by the Cambrian Flathead Sandstone (fig. 1b; Deiss, 1935).

BLACK BUTTE DEPOSIT

The strata-bound Black Butte Cu-Co-Ag Deposit occurs in the Newland Formation associated with spectacular synsedimentary pyrite-rich horizons that extend over a 25 km by 8 km area, although the main ore mineralization is localized to a fault-bounded block 8 km by 4 km (fig. 1c). Three mineralized zones occur in the lower member, which are separated stratigraphically by approximately 600 m and divided by the Volcano Valley Fault (VVF). They have been named the Johnny Lee Upper Sulfide Zone (USZ), the Lowry Middle Sulfide Zone (MSZ) and the Johnny Lee Lower Sulfide Zone (LSZ) (fig. 1b, 2; Zieg and others, 2013). The MSZ is still being studied and explored, and no samples were collected from it: this study focuses on the relatively well-characterized Johnny Lee deposits.

Petrographic analyses have shown that the mineralization within the USZ and LSZ zones is distinct texturally and mineralogically although both contain abundant early and late diagenetic pyrite and early diagenetic barite (Graham and others, 2012). Much of the early diagenetic pyrite is framboidal or occurs in small fine-grained aggregates including small circular tubes proposed to reflect pyritized microbial filaments (McGoldrick and Zieg, 2004) and chimneys (Present and others, in prep). The early diagenetic pyrite is interpreted to form from fault controlled iron-rich fluids moving through the sedimentary pile and venting at or just below the sediment surface at low temperatures (Graham and others, 2012; White and others, 2014), or from diagenetic transformations of detrital iron oxides under conditions of microbial sulfate reduction in shallow pore fluids (Schieber, 1989c). Based on framboidal textures, a general lack of base metal enrichments, and S isotopes, several authors have extended these arguments to suggest water-column precipitation of pyrite from euxinic bottom waters (Lyons and others, 2000; White and others, 2014).

A secondary diagenetic phase, especially prevalent in the USZ, formed overgrowth rims and coarse cements of pyrite. Sulfur isotope data implies the sulfur for these secondary pyrites was sourced from seawater (Zieg and Leitch, 1999). Some galena and sphalerite phases occurring in the USZ are tied to diagenetic fluids, but these minerals are not prevalent especially when compared to surrounding non-mineralized strata; Pb and Zn are not yet recognized in economic concentrations (Graham and others, 2012; White and others, 2014).

Although many Co-Ni-As-Cu rich sulfides formed relatively early during diagenesis in the USZ, a third mineralization event prior to lithification in both zones created most of the chalcopyrite as well as some chalcocite, bornite, tennenite, cobaltite, and chlorite (LSZ only) while remobilized base metals in the USZ formed siegenite (White and others, 2014). The LSZ contains a higher percentage of chalcopyrite than the USZ, although more mineralization results in a higher tonnage for the USZ. Thermodynamic calculations suggest these hydrothermal fluids were between 125°C and 225°C (White and others, 2014). In late post-lithification events, dolomite and ankerite (USZ only) precipitated within the mineralized zones (Graham and others, 2012).

METHODS

Samples from near both the USZ and LSZ were collected and analyzed to understand the richness in iron mineralization processes in the Newland Formation in this part of the Belt basin (fig 2). Twenty-five quarter-core block samples were collected in July 2013 from 4 different cores housed in the Tintina Resources, Inc. core shed, White Sulphur Springs, MT. Samples were cut using a non-magnetic brass blade into 3 cm by 2 cm billets, and made into polished thin or thick sections for further analyses. Table 1 summarizes the sample data for the 11 samples from 10 quarter-cores that were analyzed in detail.

Non-destructive rock magnetic experiments were

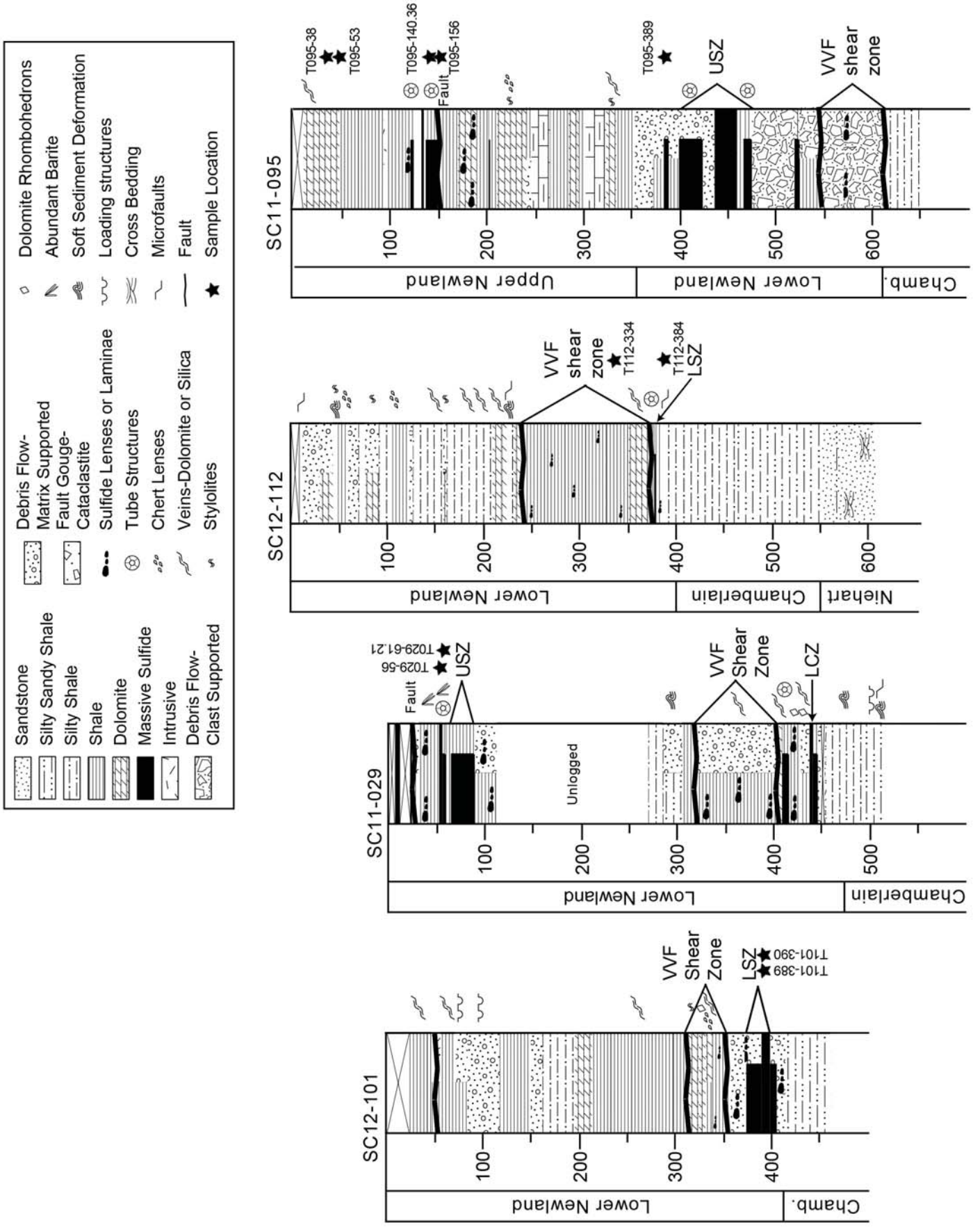

Figure 2. Lithostratigraphic columns of the drill cores from the Black Butte Deposit area examined in this study. Labeled black stars mark the stratigraphic positions of samples analyzed. Cores are not aligned by stratigraphic datum, and core depth is in meters.

Table 1: Detailed Sample Data

Sample Name	Drill Core	GPS of Drill Core Collar	Sulfide Zones	Depth of Billet (m)	Stratigraphy	Description
T029-56	SC11-029	N 46° 46' 54.8" W 110° 54' 46.33"	USZ, LSZ	56.475-56.50	Upper Newland right above USZ	Early unfilled circular tube network of iron sulfides 1-4mm in diameter with .5mm thick walls in larger massive sulfide zone
T029-61.21	SC11-029	N 46° 46' 54.8" W 110° 54' 46.33"	USZ, LSZ	61.205-61.235	Upper Newland right above USZ	Early diagenetic barite laths with differential compaction of laminated dolomitic shale with intergrown sub-parallel iron sulfide blebs rimmed with altered barite
T095-38	SC11-095	N 46° 46' 44.76" W 110° 55' 32.7"	USZ	38.70-38.76	Upper Newland far above USZ	Grey laminated silty dolomitic shale with abundant dolomite veins and iron oxide along fracture surfaces
T095-53	SC11-095	N 46° 46' 44.76" W 110° 55' 32.7"	USZ	53.50-53.56	Upper Newland far above USZ	Black laminated dolomitic shale with disseminated iron sulfides
T095-140.36	SC11-095	N 46° 46' 44.76" W 110° 55' 32.7"	USZ	140.375-140.405	Upper Newland	Early diagenetic iron sulfide nodules with differential compaction, laminae, and wavy laminae in larger massive sulfide zone, minor altered barite
T095-156	SC11-095	N 46° 46' 44.76" W 110° 55' 32.7"	USZ	156.815-156.845	Upper Newland	Large iron sulfide bleb within cross-cutting late iron sulfide band in micro-faulted grey laminated dolomitic shale
T095-389	SC11-095	N 46° 46' 44.76" W 110° 55' 32.7"	USZ	389.22-389.255	Upper Newland right above USZ	Grey laminated dolomitic shale with small debris flows and early iron sulfide broken tubes, complete to disaggregated framboids, and fine-grained laminations
T101-389	SC12-101	N 46° 46' 53.15" W 110° 54' 21.17"	LSZ	389.935-389.96	Lower Newland in LSZ	Multiple generations of cross-cutting sulfides (up to 3mm blebs) in heavily recrystallized dolomite and shale within larger massive sulfide zone
T101-390	SC12-101	N 46° 46' 53.15" W 110° 54' 21.17"	LSZ	390.085-390.11	Lower Newland in LSZ	Multiple generations of cross-cutting sulfides in heavily recrystallized dolomite and shale within larger massive sulfide zone
T112-334	SC12-112	N 46° 46' 51.53" W 110° 53' 58.67"	LSZ	334.62-334.64	Lower Newland in Volcano Valley Fault Shear Zone	Black laminated shale with disseminated iron sulfides
T112-384	SC12-112	N 46° 46' 51.53" W 110° 53' 58.67"	LSZ	384.43-334.49	Lower Newland right below LSZ	Sheared black and grey silty shale with intergrown iron sulfide blebs (<1mm) and disseminated iron sulfides

performed on thick sections or billets returned from thin sections for all 11 samples using a 2G Enterprises SQuID magnetometer following the RAPID protocols, and analyzed using the RAPID Matlab (The Mathworks, Inc.) scripts (Kirschvink and others, 2008). The RAPID protocol used here includes measurements of alternating field (AF) demagnetization of the natural remanent magnetization (NRM), anhysteretic remanent magnetization (ARM) acquisition and demagnetization, isothermal remanent magnetization (IRM) acquisition and demagnetization, backfield IRM acquisition, and rotational remanent magnetization (RRM) acquisition and demagnetization. Combined, these measurements quantify fundamental properties that can be used to distinguish different ferromagnetic minerals present in the samples (e.g. Peters and Dekkers, 2003). The destructive rock magnetic technique of KappaBridge thermal susceptibility was measured on neighboring specimens for one sample using an AGICO MFK1-FA KappaBridge and resulting data were analyzed in Matlab. Ultra-high resolution scanning SQuID Microscopy (UHRSSM) was performed on 5 of the sections with 100 μm pixels after giving them an IRM to locate and image ferromagnetic grains at the microscale.

Additional chemical imaging techniques were employed to study the non-magnetic iron- and sulfur-bearing mineral phases. Transmitted and reflected light microscopy was used to observe petrographic textures and preliminarily identify mineralogy. High-energy synchrotron-based microprobe X-ray ray fluorescence (XRF) at 13500 or 20200 eV was used to map elemental abundances with 35 μm pixels across regions in 10 representative sections at beamline 10-2 at the Stanford Synchrotron Radiation Lightsource. Additionally,

synchrotron-based X-ray near-edge absorption spectroscopy (XANES/XAS) at sulfur energies (2400-2500 eV) was paired with redox imaging at the S K-edge using a new lower energy X-ray microprobe (beamline 14-3) to collect both full spectra and multiple energy maps with 4 μm resolution and determine the mineral chemistry (oxidation state, orbital electronics, type and number of neighbors) while retaining textural information. Differences in the shape of these K-edge absorption spectra allow us to easily distinguish between a wide range of materials (Fleet, 2005; Mosselmans and others, 1995). Paired with end-member XANES spectra, the absorptions at multiple excitation energies in diagnostic regions of the XANES spectrum were collected and fit to create large maps of the mineralogy in samples. Principle component analysis of this multiple energy data was used to target and check for additional minerals. Chalcopyrite and pyrrhotite have similarities in their S K-edge spectra and thus the elemental maps made by high-energy XRF at 10-2 were used to evaluate the abundance of Cu. Synchrotron XANES and XRF analyses were performed at the Stanford Synchrotron Radiation Lightsource. Additional petrographic observations and mineral identifications were made using a ZEISS 1550VP FESEM, scanning electron microscope in the Caltech GPS Division Analytical Facility. This instrument is paired with an Oxford X-Max SDD X-ray Energy Dispersive Spectrometer (EDS) system and was used to determine X-ray spectra of elemental abundance at sub-micron sized spots on 3 thin sections to confirm the presence of chalcopyrite and galena implied from synchrotron data.

RESULTS

Rock magnetic techniques both confirmed previous observations (Graham and others, 2012; White and others, 2014) and highlighted the presence of iron mineralization not previously described in the Newland Formation shales at the Black Butte Deposit.

Rotational Remanent Magnetization (RRM)

The presence of RRM can be used to identify magnetic iron-sulfide phases like pyrrhotite, although the sensitivity limits are not well understood (Snowball, 1997; Thomson, 1990). RRM is acquired during the application of an alternating field of 90 mT (950 Hz) perpendicular to the spin axis of a sample while it is rotating at a given speed. Studies have shown that BRRM (normalized field strength of acquired RRM) varies with speed and direction of rotation so the sample is rotated clockwise and counterclockwise from 0 to 20 revolutions per second, rps (e.g. Suzuki and others, 2006). Two samples, T029-56 and T095-140.36, indicated strong evidence for magnetic iron sulfides, BRRM > ± 20 μT at 5 rps (Potter and Stephenson, 1986; Suzuki and others, 2006), while the rest of the samples showed no signs of RRM with BRRM ≈ 0 (fig. 3a). Importantly, UHRSSM imaging revealed the ferromagnetic grains in these two samples to be located in epoxy-filled holes (fig. 4cd) created either for standard emplacement of a pyrite grain for textural S isotope analyses (Present and others, in prep) or to fill porous textures when making thin sections, demonstrating that these grains are contaminants (metal alloys can produce strong RRM, Snowball, 1997). Thus, there is no evidence of magnetic iron sulfides in the Newland Formation, including the mineralized zones associated with the Black Butte Deposit.

Coercivity of Remanence Acquisition

The coercivity of remanence acquisition (Hcr'), defined as the magnetic field required to permanently flip half of the magnetic moments in a mineral, is a useful property to differentiate ferromagnetic minerals (Peters and Dekkers, 2003). Overall a measurement of how easily a mineral becomes magnetized, it is determined by taking the derivative of the acquisition of IRM curve and deconvolving the spectra into distinct peaks of different field strengths, which are the different coercivities of the mineral assemblage (Heslop and others, 2002; Robertson and France, 1994). Goethite is easily identified with coercivities over 1000 mT, and the range of 140-800 mT is unique for hematite. However, extensive data collection has shown that the coercivity ranges for hematite, magnetite, titanomagnetite, greigite and pyrrhotite overlap between 16-140 mT—though the averages of hematite (270 mT), pyrrhotite (53 mT), greigite (75 mT) are higher than those for magnetite and titanomagnetite (30 mT). Thus mineral identifications solely using Hcr' for identification have some margin of error and benefit from additional analyses (table 2).

Notably, three groups of ferromagnetic mineralogy can be separated based on Hcr' and stratigraphic/lithologic information (fig. 3b). All of the samples collected far outside the strongly mineralized sulfide zones (T095-38, T095-53, T112-334, T112-384) primarily

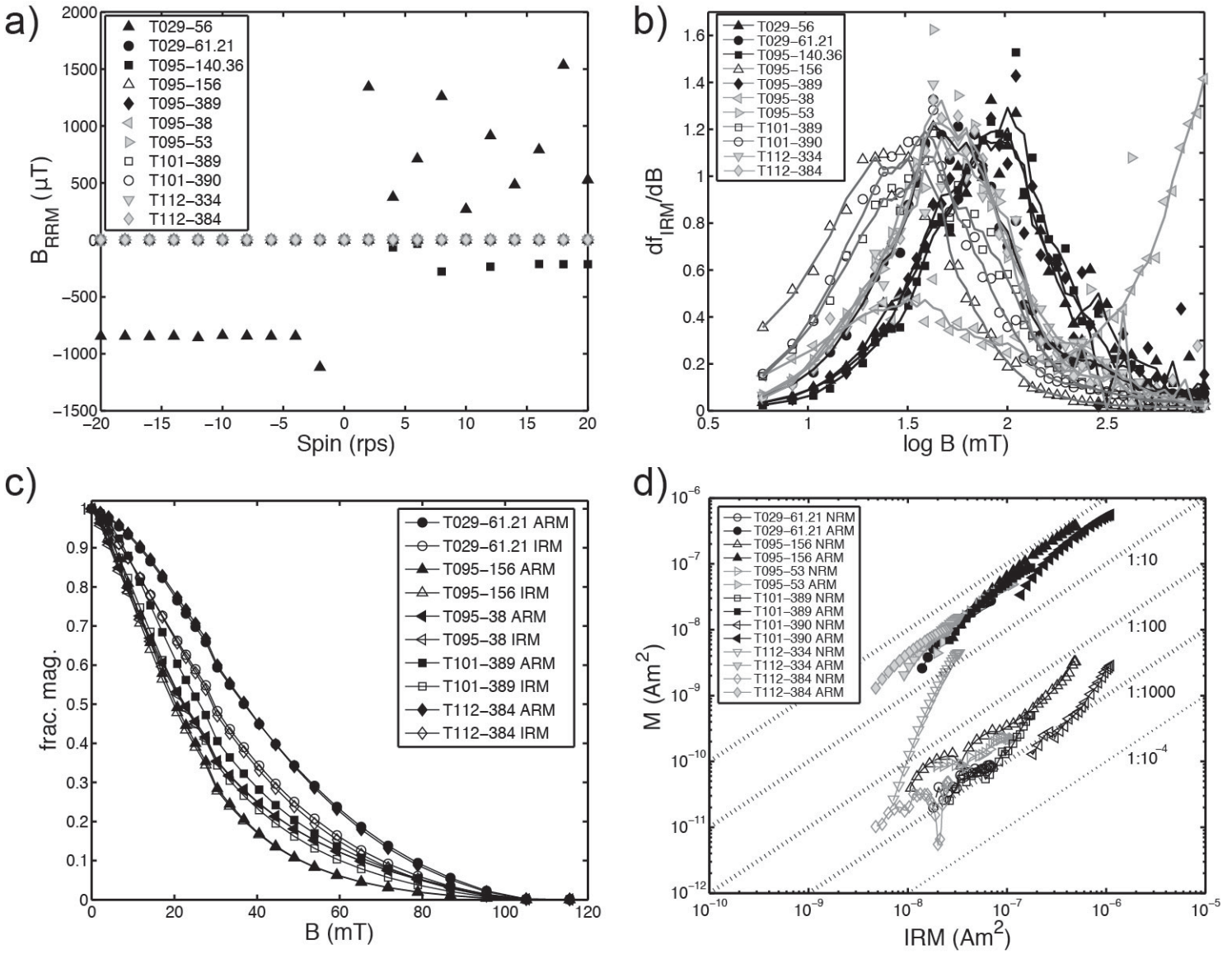

Figure 3. Rock magnetic data from shale samples of the Newland Formation. a) Rotational remanent magnetization (RRM) data to assess the presence or absence of magnetic iron sulfide phases. Negative spin speed indicated counter-clockwise rotation around the spin axis when the perpendicular alternating field is applied. All 11 samples are plotted, but only 2 of the samples are clearly visible since most of the samples have BRRM ≈ 0 at all spin speeds. b) Data showing the derivative of the isothermal remanent magnetization (IRM) of all samples to determine the coercivity of remanence (Hcr') and from this information the ferromagnetic mineralogy. The applied field (B, x-axis) at the peaks of the spectra is the Hcr'. c) Results of representative samples from the Lowrie-Fuller test to inform domain state and grain size based on the relative strength of the IRM vs. the ARM curves as measured by the fraction of total magnetization (frac. mag., Y-axis) when a specific demagnetizing field is applied (B, x-axis). d) Results from the Fuller test to provide insight into the origins (detrital, chemical, thermal) of magnetization based on the ratio of the NRM (y-axis) to IRM (x-axis). The ratio of ARM:IRM is also plotted using the same axes.

contain finely disseminated pyrite and show very similar mid-coercivity peaks interpreted to be magnetite. Sample T095-38 also shows a striking high-coercivity goethite peak; this sample contains fractures mineralized with oxides seen in hand sample and described in the core log for this stratigraphic height. Sample T029-61.21 has early diagenetic pyrite textures with minimal secondary recrystallization and contains the same magnetite mid-coercivity peak as the four samples described above. The other three samples exhibiting early diagenetic textures (T029-56, T029-140.36, T095-389), including the two samples with known ferromagnetic contamination, have slightly higher coercivity spectra. While T095-389 did not show RRM, it does have an epoxied hole with a standard, which could be contaminated by a ferromagnetic mineral/alloy similar to samples T029-140.36 and T095-389. Therefore we interpret the characteristic slightly higher Hcr' peak of these three samples to be due to contamination and not representative of early textures. Lastly, three samples display multiple generations of sulfide-bearing minerals including late displacive and

Table 2: Mineralogical Identifications from Samples of Newland Formation from Black Butte Deposit

Sample name	Bulk Techniques				S XANES and EDS							High-Energy XRF			
	Mag	Goe	Pyr	Cont	Py	Pyr	FerS	CuPy	Cov	Gal	SO4	AsPb	Cu	Zn	Ni
T029-56				X	X*			X*	X*	X*		X	X	t	
T029-61.21	X				X						X	t	X	X	
T095-38	X	X										X	X	X	t
T095-53	X				X						X	X	X	X	t
T095-140.36				X								X			
T095-156	X				X							t			
T095-389				X	X*			X*	X*	X	X	X			
T101-389	X				X		X	X				X	X	X	
T101-390	X											X	X	t	
T112-334	X				X						X	X	X	X	t
T112-384	X											t	t		t

Abbreviations: XANES = X-ray Absoption Near Edge Spectroscopy, EDS = X-ray Energy Dispersive Spectroscopy, XRF = X-ray Fluorescence, Mag = Magnetite, Goe = Goethite, Pyr = Pyrrhotite, Cont = Contamination, Py = Pyrite, FerS =Ferric Disulfide, CuPy = Chalcopyrite, Cov = Covellite, Gal = Galena, SO4 = Sulfate often Barite, AsPb = Arsenic and/or Lead

For XRF, t=trace, X = important mineral constituent

* Data from Present et al., in prep based on reflected light petrography

replacive textures (T095-156, T101-389, T101-390). These samples show a range of mid- to low-coercivity spectra suggesting larger grain size and/or multi-domain magnetite (Peters and Dekkers, 2003).

Lowrie-Fuller Test

To further examine the grain size and magnetic domain state, we employed a rock magnetic technique called the Lowrie-Fuller test—a measure of ferromagnetic grain size based on the relative stability of IRM versus ARM to applied demagnetizing AF (Lowrie and Fuller, 1971; Xu and Dunlop, 1995). In single domain grains, ARM is more stable and less easily demagnetized than IRM, while in larger multidomain grains, IRM is more stable and less easily demagnetized using AF than ARM. Although the exact physics are poorly understood, if the ARM is consistently stronger than the IRM then single domain or pseudo single domain (<10 μm) particles probably represent the majority of the magnetized minerals in a sample. While most of the samples appear to contain single-domain or pseudo-single domain particles, T095-156 (which had low coercivity spectra) does contain multi-domain grains (fig. 3c). T095-38 also is shown to contain multi-domain grains, but this sample contains goethite, which would bias the Lowrie-Fuller test toward multi-domain results. From this data, multi-domain magnetite is more common in samples with replacive textures suggesting it could have formed from recrystallization or authigenic precipitation—this can be tested if it shows a chemical remanent magnetization.

Fuller Test of NRM

Magnetite appears to be the primary ferromagnetic component in the majority of the Newland Formation shale samples. As a result, we can apply a useful rock magnetic experiment called the Fuller Test of NRM to determine if the magnetization carried by the magnetite is detrital or chemical in origin. This test uses the ratio of the NRM:IRM compared to empirical calibrations and synthetic ARM:IRM relationships of a given sample (Fuller and others, 1988; Fuller and others, 2002). Empirical calibrations on rocks with magnetite as the primary ferromagnetic mineral suggest that the weak NRM:IRM ratios of 1:1000 occur in sedimentary rocks with detrital remanent magnetization formed during primary deposition and ratios of 1:10 represents chemical remanent magnetization when magnetite has grown in situ or authigenically in a sample (Fuller and others, 2002). The ARM:IRM curve is used for comparison to demonstrate which changes in the shape of the curve are characteristic of the sample. Most samples of the Newland Formation show an NRM:IRM ratio of 1:1000, which is consistent with weak detrital remanent magnetization (fig. 3d). T112-334 shows indication of chemical remanent magneti-

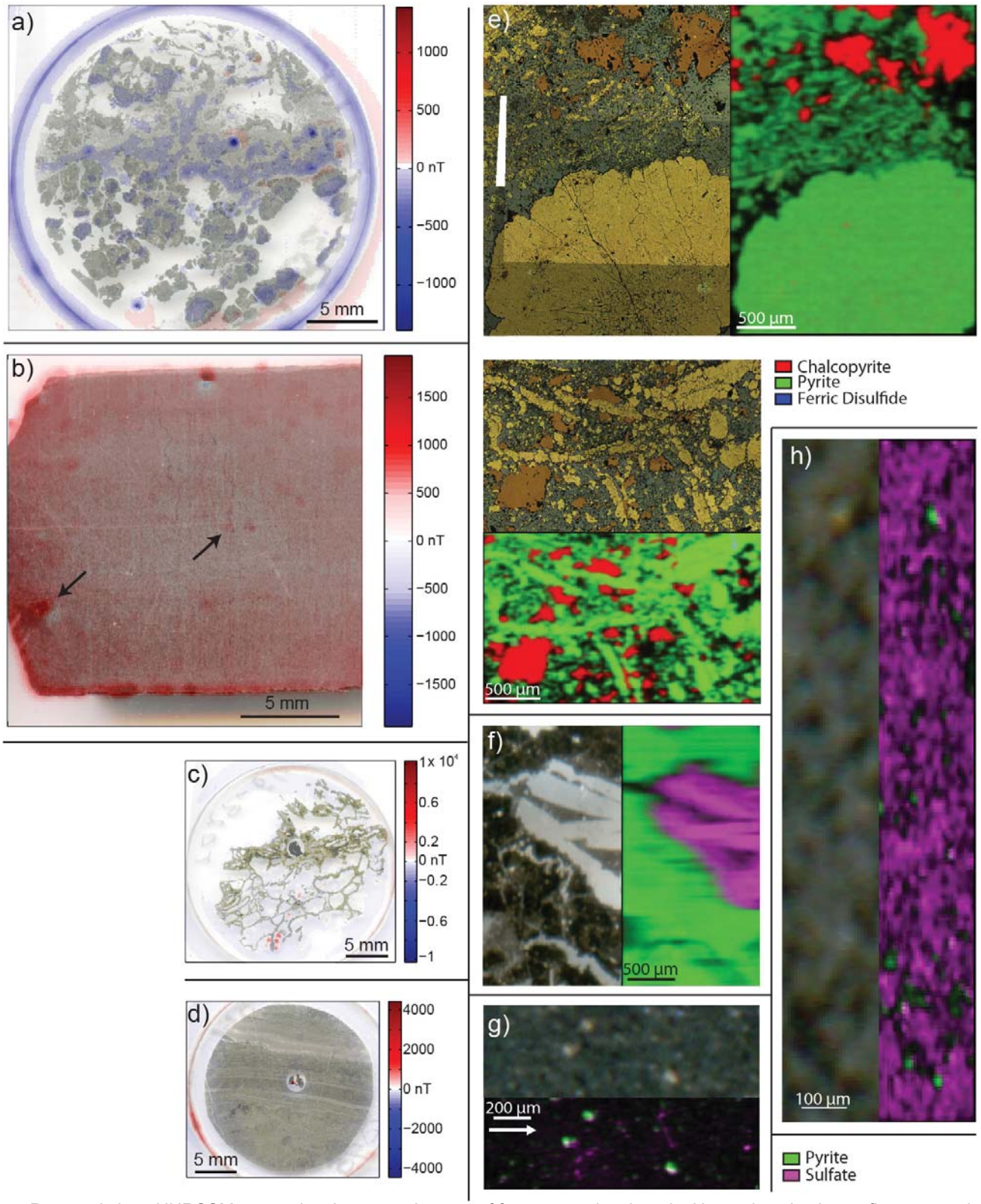

Figure 4. Parts a-d show UHRSSM magnetic microscopy images of ferromagnetic minerals. Hot and cool colors reflect magnetic vectors out of and into the page, respectively. e) Map of T101-389 showing scattered dipoles focused in fine-grained regions. f) Scattered dipoles including some that trend with post-depositional crosscutting features, such as pointed out by arrows, in T112-334. g) Image of T029-56 showing dipoles in epoxied holes around iron sulfide tube network that reflect contaminant phases introduced via standard preparation. h) Map of T095-140.36 showing single strong dipole in epoxied drill hole with pyrite standard that reflect contaminant phases introduced during preparation. Parts e-h show paired reflected light microscopy or photograph on the left-top and multiple-energy maps fit to minerals using end-member S XANES spectra on the right-bottom. Samples are oriented with correct up direction; an arrow marks the up direction for part c a) Two mapped regions of T101-389 contain multiple generations of sulfide phases including chalcopyrite, pyrite, and a unique ferric disulfide. b) Map of T026-61.21 with barite laths surrounded by early diagenetic pyrite in layers. c) Disseminated pyrite grains with associated sulfate and distinct sulfate domains in T095-53. d) Disseminated pyrite with low abundance sulfur in matrix in T112-334. Scale bar provided for each image or image pair.

zation, in which magnetite is an authigenic phase that either grew during early diagenesis or during a later diagenetic mineralization. UHRSSM maps showed the locations of disperse dipoles of ferromagnetic grains throughout samples in fine-grained material, located close to and far from secondary cross-cutting textures, consistent with a detrital origin (fig. 4a,b). However, due to the sub-micron size of these grains, the ferromagnetic minerals in the regions with dipoles could not be visualized via petrography.

KappaBridge Thermal Susceptibility

To further study the magnetite, a neighboring sample from T101-389 was used for destructive thermal susceptibility experiments using a KappaBridge. Powdered rock was slowly heated from -190°C to 700°C and then cooled to 40°C while the susceptibility from a weak induced field was measured at 20 second intervals. Susceptibility measures the ability of a sample to be magnetized in the presence of an applied field. Thus it is a magnetic measurement that integrates the entire assemblage of minerals in a sample, although ferromagnetic minerals usually dominate the signal. Changes in susceptibility during heating and cooling are produced by mineralogical transformations within the sample. A drop in susceptibility at 580°C indicates the presence of magnetite as it becomes paramagnetic at its Curie temperature (fig. 5a). The low-temperature Verwey transition typical for magnetite at -150°C as it transforms from weakly magnetic monoclinic magnetic structure and to ferromagnetic cubic structure was not observed in this sample; either it was suppressed due to low abundance with other phases dominating the signal, or the magnetite contains a small weight percent titanium (Kozłowski and others, 1996; Moskowitz and others, 1998). A slight drop in susceptibility at 80°C is suggestive of goethite decomposing and reacting with sulfur to form pyrite or decomposition of titanomagnetite (Charilaou and others, 2011; Minyuk and others, 2013). Although the typical pyrite/chalcopyrite decomposition peak to magnetite is not seen (Li and Zhang, 2005; Minyuk and others, 2013), some new magnetite and a substantial amount of pyrrhotite were formed after heating to 700°C in an argon atmosphere based on the fact that the cooling curves increase in susceptibility during cooling with distinct peaks at 580°C and at 320°C the respective Curie temperatures for those minerals (fig. 5b). The creation of these minerals suggests there were non-magnetic iron sulfides in these samples that transformed into magnetic minerals during the heating process.

X-Ray Spectroscopy

Iron sulfide phases were visually identified in all of the samples using light microscopy. We used X-ray spectroscopy, specifically XANES and XRF, to evaluate the exact chemical composition and crystal structure of these phases (table 2). Ferrous disulfide was identified as the major sulfide-bearing phase in all the samples (fig. 6). The ferrous disulfide minerals marcasite and pyrite have similar S K-edge spectra

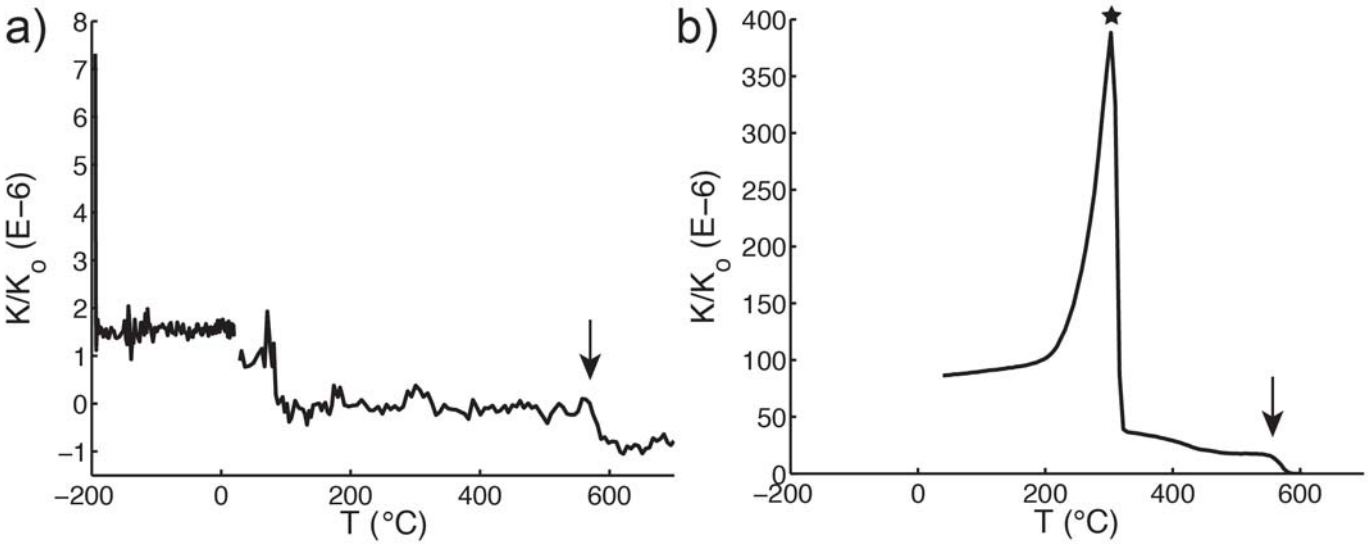

Figure 5. KappaBridge results for a representative shale sample, T101-389. a) Magnetic susceptibility during heating from -190°C to 700°C. b) Magnetic susceptibility during cooling from 700°C to 23°C. Note the different y-axis scale as there is increased susceptibility during this cooling phase. Data are normalized to the blank, an empty specimen holder measurement. Arrows mark the Curie temperature of magnetite (580°C) while the star marks the Curie temperature of pyrrhotite (320°C).

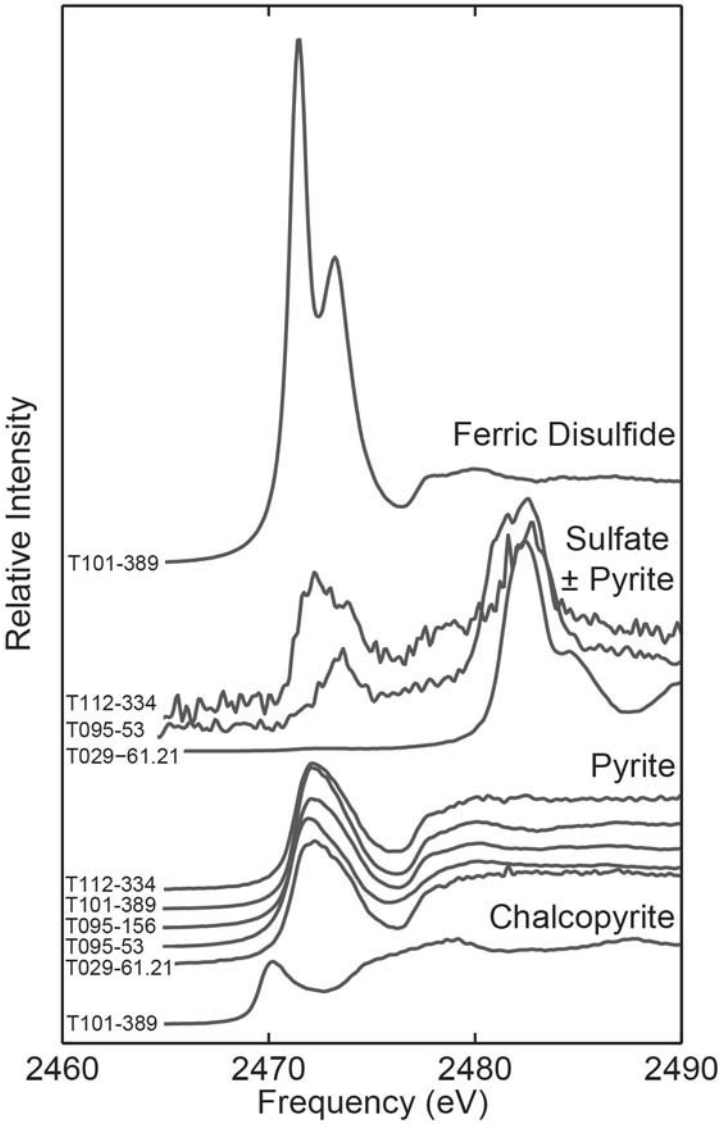

Figure 6. Synchrotron S K-edge XANES spectra for phases identified in all samples. An unnamed unique mineral, a ferric disulfide not previously found in natural samples, is identified based off its K-edge spectra, which shows Fe+3 bonding with di-sulfide valence sulfur.

using XANES and can only be readily distinguished by the Fe L-edge (Mosselmans and others, 1995) or X-ray diffraction, which were not measured here. However, petrography shows that the disulfides phases present in these samples are pyrite. Chalcopyrite was observed as a major component of T101-389 (fig. 4e, 6). Sulfate salts were also identified in many of the samples including laths of barite that show differential compaction of sedimentary laminae (fig. 4f, 6). However, in the samples with disseminated pyrite, small domains of sulfate (10-20 μm in size) were found both alone and associated with pyrite, suggesting some of the sulfate minerals could be iron sulfates instead of barite (fig. 4g,h, 6). EDS and high-energy XRF maps were used to confirm the presence of chalcopyrite (as opposed to pyrrhotite); however, the XRF maps also highlight interesting patterns in base metal mineralization. Some replacive pyrite grains contain greater amounts of As, Pb, Zn, or Cu (fig. 7 d,e,g), while other regions hosted chalcophile metals as dominant cations in sulfide phases like Cu in chalcopyrite (fig. 7a-f,h). Microprobe X-ray spectroscopy paired mapping capabilities, coupled with traditional petrographic and bulk chemical techniques, provide an exciting new tool for mineral analysis opening new avenues for inquiry into trace metal abundances, redox states and gradients, and mineral phase identification.

DISCUSSION AND CONCLUSIONS

Bulk rock magnetic techniques employed in this study confirm the absence of pyrrhotite in shales of the Newland Formation near the Black Butte Deposit, in contrast to its ubiquitous presence in correlative units at higher metamorphic grades to the northwest (Slotznick and others, in review). This result confirms that these rocks have not been heated to very high temperatures, and while hydrothermal fluids did cause overprinting and recrystallization of sulfide phases, no pyrrhotite was formed with this mineralization. This is important for bulk geochemical studies such as iron speciation (Planavsky and others, 2011) because pyrrhotite may be misplaced in sequential chemical extraction with the magnetite fraction and/or result in incorrect iron calculations due to its unique chemistry during the pyrite extraction—both could make a basin appear more ferruginous than it was by incorrectly identifying the iron mineralogy (Asael and others, 2013; Schumann and others, 2012)). Samples collected far outside the massive sulfide mineralization zones contain early diagenetic disseminated pyrite grains (Schieber, 1989a); copper, zinc, and lead sulfides are rare in these areas but their presence still signals some mineralization extends beyond the regions of economic interest. Sulfide phases tied to these hydrothermal fluids should be taken into account when using Belt strata to interpret the ancient redox conditions and processes operating in the Belt Basin, because these phases show iron was mobile and likely advected from elsewhere in the sediment pile. The hydrothermal fluids could have also sourced iron for some of the magnetite present in the samples and/or been responsible for recrystallization processes.

The identification of magnetite in Newland Formation shales provides important insights into the redox

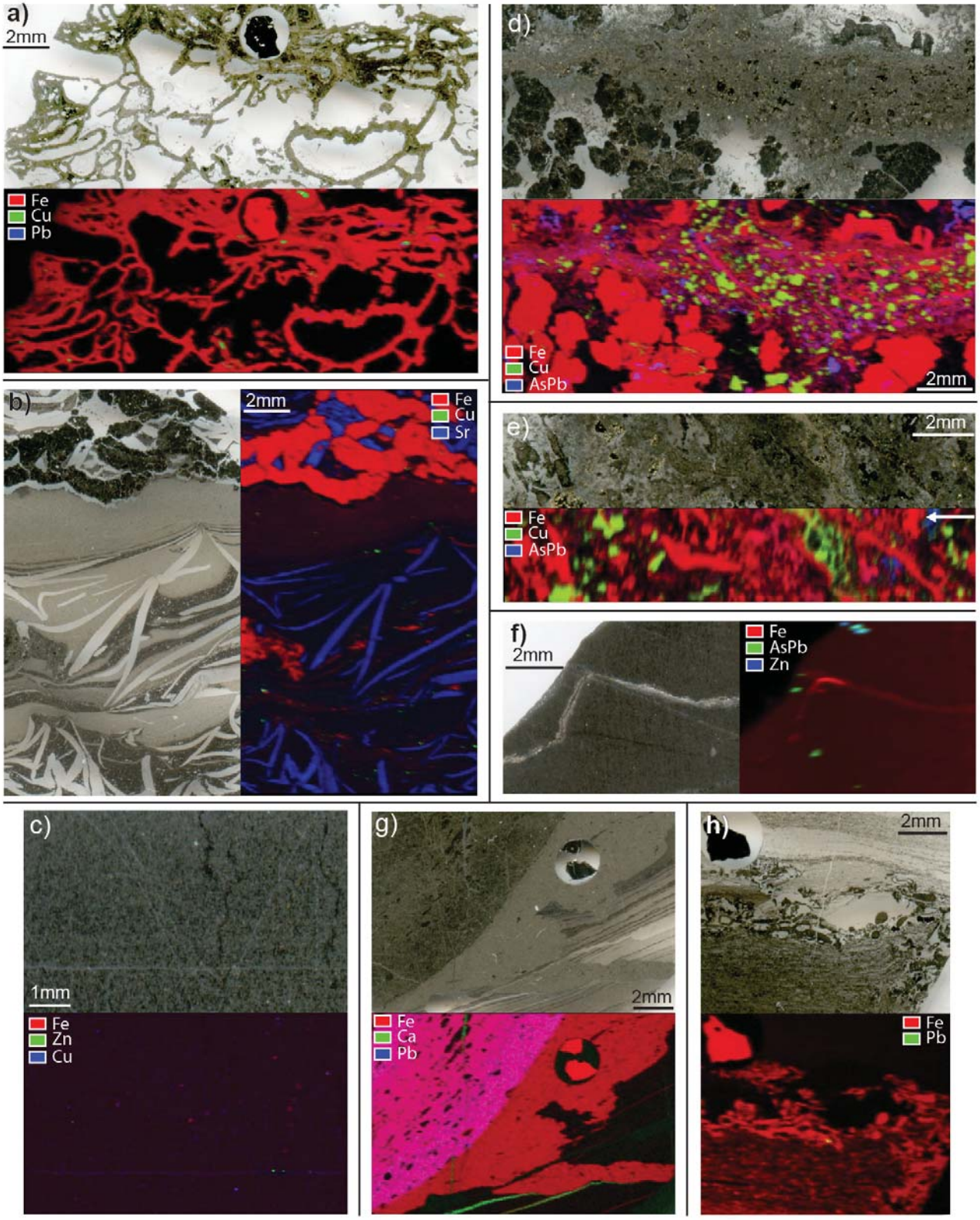

Figure 7. High-Energy XRF maps of metal abundances (right-bottom) shown alongside a light scan of a given sample in thick or thin section (left-top). Samples are oriented with correct up direction; an arrow marks the up direction for part e. a) Unfilled tubular network of iron sulfide cements with small inclusions of Pb- and Cu-bearing minerals in T029-56. b) Early diagenetic and recrystallized barite containing trace Sr with sub-parallel pyrite blebs and small Cu-bearing minerals in T029-61.21. c) Disseminated pyrite with distinct Zn and Cu minerals that show mineralization associated both along lamination and crosscutting features in T112-334. d) Multiple generations of sulfides including pyrite and chalcopyrite with As- and Pb-rich grains, zones of finely disseminated grains, and zones within euhedral grains in T101-389 e) Closer look at multiple generations of iron sulfides and chalcopyrite with As- and Pb-rich grains and zones in larger grains in T101-390. f) Dolomite vein containing iron oxide with As-, Pb-, and Zn-rich minerals associated with smaller non-dolomitized fractures and/or laminations in T095-38. g) Vertical dolomitic veins cut Pb-rich pyrite bleb within a crosscutting pyrite aggregate in a laminated dolomitic shale in T095-156. h) Intraformational detrital iron sulfides parallel to, and deforming shale laminates with small amounts of galena in T095-389.

character and mode of iron delivery in this part of the Belt Basin. Rock magnetic experiments indicate that magnetite is primarily detrital in origin, with limited evidence for authigenic magnetite in some samples. Though pyrite is commonly the most abundant iron-bearing mineral present in these diagenetically stabilized lithologies, detrital magnetite represents an important sedimentary vector for iron delivery to this basin that is not a direct measure of redox conditions in seawater. Furthermore, detrital iron oxides might bias iron speciation data toward compositions that appear more anoxic and ferruginous (Planavsky and others, 2011); during deposition Belt Basin waters could have either been more oxic or more euxinic depending on the relative abundances of these oxides and other iron-bearing minerals. Petrography and X-ray imaging reveal that pyrite is ever-present as small framboids and disseminated grains exhibiting textures that are consistent with the formation of much of this pyrite in the water column or in sediments during early diagenesis (Graham and others, 2012; Schieber, 1989a; Wilkin and others, 1996). We speculate that detrital iron oxides were an important source of reactive iron for early pyrite formation (e.g. Canfield and Berner, 1987; Reynolds and others, 2000; Schieber, 1989c). Many samples (not just limited to economically meaningful sulfide mineralization zones) show additional sulfide phases in late diagenetic textures that mark iron sourced by hydrothermal fluids. If iron sources did not limit early pyrite formation more broadly, perhaps this was limited by the abundance of H2S in the bottom water, bacterial sulfate reduction/sulfur oxidation rates, and/or sedimentation rates. More work is needed to better understand the interplay between these factors (Present and others, in prep), but what is clear at present is that we do not see clear evidence for the ferruginous water column conditions during the depositional of Newland Formation shales put forward on the basis of iron speciation data (Planavsky and others, 2011).

Based on our observations, we hypothesize that bottom waters in Helena Embayment during the deposition of the Newland Formation were suboxic or possibly euxinic (Gellatly and Lyons, 2005; Lyons and others, 2000), and that detrital fluxes played an important role in delivery of iron into the Helena Embayment, much of which was transformed into pyrite during sulfate reduction associated with early diagenesis of these organic-rich sediments (Lyons and others, 2000; Strauss and Schieber, 1990). This is a similar mode of iron deposition and pyrite production today in modern euxinic basins and anoxic pore waters in marine sediments (e.g. Berner, 1984), and implies a degree of continuity of redox conditions and processes operating in large sedimentary basins over the past one and a half billion years.

ACKNOWLEDGMENTS

We thank John Grotzinger, Ted Present, Andy Knoll, Ken Williford and the members of the 2013 Agouron Field Course for assistance with sample collection. Support for this work was provided by the Agouron Institute, Tobacco Root Geological Society Scholarship, Belt Association Student Research Grant, the David and Lucile Packard Foundation (W.W.F.), NSF Graduate Research Fellowship program (S.P.S.), and NASA Earth and Space Fellowship (S.P.S.). Portions of this research were carried out at the Stanford Synchrotron Radiation Lightsource, a Directorate of SLAC National Accelerator Laboratory and an Office of Science User Facility operated for the U.S. Department of Energy Office of Science by Stanford University.

REFERENCES

Asael, D., Tissot, F. L., Reinhard, C. T., Rouxel, O., Dauphas, N., Lyons, T. W., Ponzevera, E., Liorzou, C., and Chéron, S., 2013, Coupled molybdenum, iron and uranium stable isotopes as oceanic paleoredox proxies during the Paleoproterozoic Shunga Event: Chemical Geology, v. 362, p. 193-210.

Berner, R. A., 1984, Sedimentary pyrite formation: an update: Geochimica et Cosmochimica Acta, v. 48, no. 4, p. 605-615.

Brocks, J. J., Buick, R., Summons, R. E., and Logan, G. A., 2003, A reconstruction of Archean biological diversity based on molecular fossils from the 2.78 to 2.45 billion-year-old Mount Bruce Supergroup, Hamersley Basin, Western Australia: Geochimica et Cosmochimica Acta, v. 67, no. 22, p. 4321-4335.

Canfield, D., 1998, A new model for Proterozoic ocean chemistry: Nature, v. 396, no. 6710, p. 450-453.

Canfield, D. E., and Berner, R. A., 1987, Dissolution and pyritization of magnetite in anoxie marine

sediments: Geochimica et Cosmochimica Acta, v. 51, no. 3, p. 645-659.

Charilaou, M., Löffler, J., and Gehring, A., 2011, Fe–Ti-O exchange at high temperature and thermal hysteresis: Geophysical Journal International, v. 185, no. 2, p. 647-652.

Cloud, P. E., 1968, Atmospheric and Hydrospheric Evolution on the Primitive Earth: Science, v. 160, no. 3829, p. 729-736.

Craig, J. R., and Vokes, F. M., 1993, The metamorphism of pyrite and pyritic ores: an overview: Mineralogical Magazine, v. 57, no. 1, p. 3-18.

Deiss, C., 1935, Cambrian-Algonkian unconformity in western Montana: Geological Society of America Bulletin, v. 46, no. 1, p. 95-124.

Duke, E. F., and Lewis, R. S., 2010, Near infrared spectra of white mica in the Belt Supergroup and implications for metamorphism: American Mineralogist, v. 95, no. 7, p. 908-920.

Embley, T. M., and Martin, W., 2006, Eukaryotic evolution, changes and challenges: Nature, v. 440, no. 7084, p. 623-630.

Fleet, M. E., 2005, XANES spectroscopy of sulfur in earth materials: The Canadian Mineralogist, v. 43, no. 6, p. 1811-1838.

Fuller, M., Kidane, T., and Ali, J., 2002, AF demagnetization characteristics of NRM, compared with anhysteretic and saturation isothermal remanence: an aid in the interpretation of NRM: Physics and Chemistry of the Earth, v. 27, no. 25-31, p. 1169-1177.

Gellatly, A. M., and Lyons, T. W., 2005, Trace sulfate in mid-Proterozoic carbonates and the sulfur isotope record of biospheric evolution: Geochimica et Cosmochimica Acta, v. 69, no. 15, p. 3813-3829.

Graham, G., Hitzman, M. W., and Zieg, J., 2012, Geologic Setting, Sedimentary Architecture, and Paragenesis of the Mesoproterozoic Sediment-Hosted Sheep Creek Cu-Co-Ag Deposit, Helena Embayment, Montana: Economic Geology, v. 107, no. 6, p. 1115-1141.

Hall, A. J., 1986, Pyrite-pyrrhotine redox reactions in nature: Mineralogical Magazine, v. 50, p. 223-229.

Harrison, J. E., 1972, Precambrian Belt basin of northwestern United States: Its geometry, sedimentation, and copper occurrences: Geological Society of America Bulletin, v. 83, no. 5, p. 1215-1240.

Heslop, D., Dekkers, M., Kruiver, P., and Van Oorschot, I., 2002, Analysis of isothermal remanent magnetization acquisition curves using the expectation-maximization algorithm: Geophysical Journal International, v. 148, no. 1, p. 58-64.

Holland, H. D., 1984, The chemical evolution of the atmosphere and oceans, Princeton University Press.

Holland, H.D., 2006, The oxygenation of the atmosphere and oceans: Philosophical Transactions of the Royal Society B: Biological Sciences, v. 361, no. 1470, p. 903-915.

Horodyski, R. J., Winston, D., and Whipple, J. W., 1989, Paleontology of the middle Proterozoic belt supergroup, *in* Winston, D., Horodyski, R. J., and Whipple, J. W., eds., Middle Proterozoic Belt Supergroup, Western Montana: Great Falls, Montana to Spokane, Washington: 28th International Geological Congress, Field Trip Guidebook T334, p. 7-26.

Kirschvink, J. L., Kopp, R. E., Raub, T. D., Baumgartner, C. T., and Holt, J. W., 2008, Rapid, precise, and high-sensitivity acquisition of paleomagnetic and rock-magnetic data: Development of a low-noise automatic sample changing system for superconducting rock magnetometers: Geochemistry Geophysics Geosystems, v. 9, no. 5.

Knoll, A. H., Javaux, E. J., Hewitt, D., and Cohen, P., 2006, Eukaryotic organisms in Proterozoic oceans: Philosophical Transactions of the Royal Society B: Biological Sciences, v. 361, no. 1470, p. 1023-1038.

Kozłowski, A., Kakol, Z., Kim, D., Zalecki, R., and Honig, J., 1996, Heat capacity of Fe 3-α M α O 4 (M= Zn, Ti, $0 \leqslant \alpha \leqslant 0.04$): Physical Review B, v. 54, no. 17, p. 12093.

Li, H. Y., and Zhang, S. H., 2005, Detection of Mineralogical Changes in Pyrite Using Measurements of Temperature-Dependence Susceptibilities: Chinese Journal of Geophysics, v. 48, no. 6, p. 1454-1461.

Lowrie, W., and Fuller, M., 1971, Alternating field demagnetization characteristics of multidomain thermoremanent magnetization in magnetite:

Journal of Geophysical Research, v. 76, no. 26, p. 6339-&.

Luepke, J. J., 1999, Goechemical trends in shales of the Belt Supergroup, Northwestern US: a marine model for the evolution of the Mesoproterozoic weatern Laurentian Margin [M.S. thesis: University Missouri-Columbia, 133 p.

Luepke, J. J., and Lyons, T. W., 2001, Pre-Rodinian (Mesoproterozoic) supercontinental rifting along the western margin of Laurentia: geochemical evidence from the Belt-Purcell Supergroup: Precambrian Research, v. 111, no. 1, p. 79-90.

Lyons, T. W., Luepke, J. J., Schreiber, M. E., and Zieg, G. A., 2000, Sulfur geochemical constraints on Mesoproterozoic restricted marine deposition: lower Belt Supergroup, northwestern United States: Geochimica et Cosmochimica Acta, v. 64, no. 3, p. 427-437.

McGoldrick, P., and Zieg, J., Massive microbes from the Mesoproterozoic of Montana, *in* Proceedings 17th Australia Geological Geological Convention Hobart, Australia, 2004, Volume 73, p. 100.

Minyuk, P., Tyukova, E., Subbotnikova, T., Kazansky, A. Y., and Fedotov, A., 2013, Thermal magnetic susceptibility data on natural iron sulfides of northeastern Russia: Russian Geology and Geophysics, v. 54, no. 4, p. 464-474.

Moreau, M., Ader, M., and Enkin, R., 2005, The magnetization of clay-rich rocks in sedimentary basins: low-temperature experimental formation of magnetic carriers in natural samples: Earth and Planetary Science Letters, v. 230, no. 1, p. 193-210.

Moskowitz, B. M., Jackson, M., and Kissel, C., 1998, Low-temperature magnetic behavior of titanomagnetites: Earth and Planetary Science Letters, v. 157, no. 3, p. 141-149.

Mosselmans, J., Pattrick, R., Van der Laan, G., Charnock, J., Vaughan, D., Henderson, C., and Garner, C., 1995, X-ray absorption near-edge spectra of transition metal disulfides FeS2 (pyrite and marcasite), CoS2, NiS2 and CuS2, and their isomorphs FeAsS and CoAsS: Physics and Chemistry of Minerals, v. 22, no. 5, p. 311-317.

Mudge, M. R., Erickson, R. L., Kleinkopf, M. D., and Zartman, R. E., 1968, Reconnaissance geology, geophysics, and geochemistry of the southeastern part of the Lewis and Clark Range, Montana.

Nelson, W. H., 1963, Geology of the Duck Creek Pass quadrangle, Montana, U.S. Geological Survey Bulletin, Volume 1121-J, p. 56.

Peters, C., and Dekkers, M., 2003, Selected room temperature magnetic parameters as a function of mineralogy, concentration and grain size: Physics and Chemistry of the Earth, Parts A/B/C, v. 28, no. 16, p. 659-667.

Planavsky, N. J., McGoldrick, P., Scott, C. T., Li, C., Reinhard, C. T., Kelly, A. E., Chu, X., Bekker, A., Love, G. D., and Lyons, T. W., 2011, Widespread iron-rich conditions in the mid-Proterozoic ocean: Nature, v. 477, no. 7365, p. 448-451.

Potter, D., and Stephenson, A., 1986, The detection of fine particles of magnetite using anhysteretic and rotational remanent magnetizations: Geophysical Journal International, v. 87, no. 2, p. 569-582.

Poulton, S. W., and Canfield, D. E., 2005, Development of a sequential extraction procedure for iron: implications for iron partitioning in continentally derived particulates: Chemical Geology, v. 214, no. 3, p. 209-221.

Poulton, S.W., and Canfield, D.E., 2011, Ferruginous conditions: a dominant feature of the ocean through Earth's history: Elements, v. 7, no. 2, p. 107-112.

Present, T. M., Slotznick, S. P., Creveling, J. R., Bergmann, K. D., Meyers, C. E., Williford, K. H., Fischer, W. W., Knoll, A. H., Grotzinger, J. P., and A., Z. G., in prep, Porous macroscopic pyrite networks in a Mesoproterozoic SEDEX massive sulfide deposit.

Raub, T., Johnson, S. C., and Raub, T. D., 2012, Rock magnetic detection of the pyrite-to-pyrrhotite reduction: applications to hydrocarbon maturity, mineral resources, and biogeochemistry, American Geophysical Union, Fall Meeting: San Francisco, CA, p. GP34A-08.

Raymond, J., and Blankenship, R. E., 2004, Biosynthetic pathways, gene replacement and the antiquity of life: Geobiology, v. 2, no. 4, p. 199-203.

Reynolds, R. L., Rosenbaum, J. G., Sweetkind, D. S., Lanphere, M. A., Roberts, A. P., and Verosub, K. L., 2000, Recognition of primary and diagenetic magnetizations to determine the magnetic polarity record and timing of deposition of the moat-fill

rocks of the Oligocene Creede Caldera, Colorado: Geological Society of America Special Papers, v. 346, p. 77-93.

Robertson, D., and France, D., 1994, Discrimination of remanence-carrying minerals in mixtures, using isothermal remanent magnetisation acquisition curves: Physics of the Earth and Planetary Interiors, v. 82, no. 3, p. 223-234.

Ross, G. M., and Villeneuve, M., 2003, Provenance of the Mesoproterozoic (1.45 Ga) Belt basin (western North America): Another piece in the pre-Rodinia paleogeographic puzzle: Geological Society of America Bulletin, v. 115, no. 10, p. 1191-1217.

Schieber, J., 1989a, Facies and origin of shales from the mid-Proterozoic Newland Formation, Belt Basin, Montana, USA: Sedimentology, v. 36, no. 2, p. 203-219.

Schieber, J., 1989b, The origin of the Neihart Quartzite, a basal deposit of the Mid-Proterozoic Belt Supergroup, Montana, USA: Geological Magazine, v. 126, no. 03, p. 271-281.

Schieber, J., 1989c, Pyrite mineralization in microbial mats from the mid-Proterozoic Newland Formation, Belt Supergroup, Montana, USA: Sedimentary geology, v. 64, no. 1, p. 79-90.

Schumann, R., Stewart, W., Miller, S., Kawashima, N., Li, J., and Smart, R., 2012, Acid–base accounting assessment of mine wastes using the chromium reducible sulfur method: Science of the Total Environment, v. 424, p. 289-296.

Slotznick, S. P., Winston, D., Webb, S. M., Kirschvink, J. L., and Fischer, W. W., in review, Iron mineralogy and redox conditions during deposition of the Mesoproterozoic Appekunny Formation, Belt Supergroup, Glacier National Park Geological Society of America Special Paper.

Snowball, I. F., 1997, The detection of single-domain greigite (Fe3S4) using rotational remanent magnetization (RRM) and the effective gyro field (Bg): mineral magnetic and palaeomagnetic applications: Geophysical Journal International, v. 130, no. 3, p. 704-716.

Strauss, H., and Schieber, J., 1990, A sulfur isotope study of pyrite genesis: the Mid-Proterozoic Newland Formation, Belt Supergroup, Montana: Geochimica et Cosmochimica Acta, v. 54, no. 1, p. 197-204.

Stüeken, E. E., 2013, A test of the nitrogen-limitation hypothesis for retarded eukaryote radiation: nitrogen isotopes across a Mesoproterozoic basinal profile: Geochimica et Cosmochimica Acta, v. 120, p. 121-139.

Suzuki, Y., Kopp, R. E., Kogure, T., Suga, A., Takai, K., Tsuchida, S., Ozaki, N., Endo, K., Hashimoto, J., and Kato, Y., 2006, Sclerite formation in the hydrothermal-vent "scaly-foot" gastropod—possible control of iron sulfide biomineralization by the animal: Earth and Planetary Science Letters, v. 242, no. 1, p. 39-50.

Thomson, G. F., 1990, The anomalous demagnetization of pyrrhotite: Geophysical Journal International, v. 103, no. 2, p. 425-430.

Walcott, C. D., 1899, Pre-Cambrian fossiliferous formations: Geological Society of America Bulletin, v. 10, no. 1, p. 199-244.

Walter, M., Oehler, J. H., and Oehler, D. Z., 1976, Megascopic algae 1300 million years old from the Belt Supergroup, Montana: a reinterpretation of Walcott's Helminthoidichnites: Journal of Paleontology, p. 872-881.

White, J., Gammons, C. H., and Zieg, G., 2014, Paragenesis of cobalt and nickel in the Black Butte shale-hosted copper deposit, Belt Basin, Montana, USA: Mineralium Deposita, v. 49, no. 3, p. 335-351.

Wilkin, R., Barnes, H., and Brantley, S., 1996, The size distribution of framboidal pyrite in modern sediments: an indicator of redox conditions: Geochimica et Cosmochimica Acta, v. 60, no. 20, p. 3897-3912.

Winston, D., and Link, P., 1993, Middle Proterozoic rocks of Montana, Idaho and eastern Washington: the Belt Supergroup: Precambrian: Conterminous US: The Geology of North America, v. 2, p. 487-517.

Xu, S., and Dunlop, D. J., 1995, Toward a better understanding of the Lowrie-Fuller test: Journal of Geophysical Research: Solid Earth (1978–2012), v. 100, no. B11, p. 22533-22542.

Zieg, G., and Leitch, C., The geology of the Sheep Creek copper deposit, Meagher County, Montana, *in* Proceedings Belt Symposium III Abstracts, 1993: Montana Bureau of Mines and Geology1999, Volume 381.

Zieg, G., Scartozzi, V., Chutas, N., Albers, D., Gostomski, K., and Jones, J., 2013, Black Butte copper deposits, lower Belt Supergroup, Montana: Northwest Geology, v. 42, p. 131-147.

Zieg, G. A., 1986, Stratigraphy and sedimentology of the Middle Proterozoic Newland Limestone: Montana Bureau of Mines and Geology Special Publication, v. 94, p. 125-141.